

Direct removal of edge-localized pollutant emission in a near-infrared bremsstrahlung measurement

J. K. Anderson,^{a)} P. L. Andrew,^{b)} B. E. Chapman, D. Craig, and D. J. Den Hartog
Department of Physics, University of Wisconsin, 1150 University Avenue, Madison, Wisconsin 53706

(Presented on 10 July 2002)

Visible and near-infrared electron-ion bremsstrahlung measurements in fusion research devices, used to determine the effective ionic charge (Z_{eff}), are often plagued by pollutant emission from the cool-edge region. The primary sources of visible and near-infrared non-bremsstrahlung continuum emission in the Madison Symmetric Torus arise from electron-neutral interactions, and the pollutant emission is hence directly proportional to the bulk neutral density. Simultaneously monitoring the total emission at 1040 nm and the neutral contaminant (via D_{α} emission) has enabled an extraction of the electron-ion bremsstrahlung and a measurement of Z_{eff} at comparatively low electron density (10^{13} cm^{-3}). © 2003 American Institute of Physics. [DOI: 10.1063/1.1537440]

I. INTRODUCTION

The effective ionic charge (Z_{eff}) is a measure of the plasma contamination from impurities and has broad-ranging consequences, as it determines, in part, the plasma resistivity, ohmic heating efficiency, and total radiated power. Continuous electron-ion (e-i) bremsstrahlung emission, arising from Coulomb collisions between electrons and ions, can be used to measure the effective ionic charge, as the emissivity at a given wavelength λ is

$$\epsilon_{e-i}(\lambda) = 1.516 \times 10^{-30} \frac{\bar{g}_{\text{ff}} n_e^2 Z_{\text{eff}} e^{-hc/\lambda k T_e}}{\lambda^2 \sqrt{T_e}} \left[\frac{\text{W}}{\text{cm}^3 \text{ nm sr}} \right], \quad (1)$$

where T_e is the electron temperature (in eV), n_e is the electron density, and \bar{g}_{ff} is the free-free Gaunt factor. The effective ionic charge is

$$Z_{\text{eff}} = \frac{\sum_s n_s Z_s^2}{\sum_s n_s Z_s} = \frac{\sum_s n_s Z_s^2}{n_e}, \quad (2)$$

where n_s is the density, Z_s is the charge state, and the summation is over all ionic species present in the plasma.

Accurate deduction of Z_{eff} is possible with an absolutely calibrated measurement of the emissivity (and electron density and temperature) in a wavelength region where e-i bremsstrahlung is the dominant source of light. Identification of wavelength regions free of atomic lines and other radiation is challenging, but successful bremsstrahlung measurements have been made on several fusion research devices in the visible range near 523 nm¹⁻⁵ and 536 nm,^{6,7} and in the near-infrared (NIR) near 980 nm⁸ and 1040 nm.⁹⁻¹¹ These measurements are challenging, as molecular pseudocontinua⁷ and generic recycling light contribute to the total emission and are difficult to quantify and to remove. Due to the n_e^2 dependence of bremsstrahlung, the sensitivity to pollutant

light is magnified in the typically low-density ($n_e \sim 1 \times 10^{13} \text{ cm}^{-3}$) Madison Symmetric Torus (MST) plasmas. The expected emission is decreased significantly compared to that reported in Refs. 2-12, with densities in the mid-to-upper 10^{13} cm^{-3} range. In this work, we have identified the primary pollutants in the visible-to-NIR range, and report significant emission from electron-neutral (e-n) bremsstrahlung in relatively high-temperature fusion research plasmas. Emission from dissociation of the deuterium molecule prohibits a visible bremsstrahlung measurement in MST, but direct removal of the contaminant emission from neutrals has enabled a measurement of core NIR bremsstrahlung emission in high-temperature [$T_e(0) \sim 800 \text{ eV}$] MST plasmas.

The diagnostic used to simultaneously measure the NIR and D_{α} emission is shown in Fig. 1, where 17 poloidal viewing chords accommodate an array of detectors. The three-lens optical system detailed in the inset samples a cylindrical volume, and appropriate filters select the desired wavelength of collection. At the focal point of the optics is a silicon photodiode whose output is amplified and sampled at 100 kHz. A common BK7 microscope slide is used as a partially reflecting surface ($R \lesssim 10\%$), directing a small fraction of the incident light onto a D_{α} detector while transmitting the majority of the light onto an NIR detector. Calibration of the detectors is performed with optics and a viewing geometry identical to that on the MST. Eight viewing chords are outfitted with the colinear detector pairs for a modestly resolved profile diagnostic.

II. POLLUTANT EMISSION

The validity of an e-i bremsstrahlung measurement hinges on minimization of pollutants. Visible bremsstrahlung measurements on MST have proven unsuccessful, as the measured continuum, shown in Fig. 2, overwhelms the bremsstrahlung expected for $Z_{\text{eff}}=2$. Emission levels in apparently line-free regions (near 480 or 523 nm) are explainable only by bremsstrahlung with unrealistically high Z_{eff} values of 20 to 60, implying that other sources of emission are dominant.

^{a)}Electronic mail: jkanders@facstaff.wisc.edu

^{b)}Current address: EURATOM-UKAEA Fusion Assoc., Culham Science Centre, Abingdon, Oxfordshire OX14 3EA, United Kingdom.

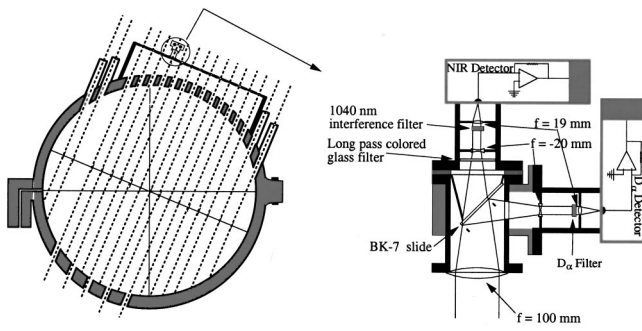


FIG. 1. Poloidal cross section of MST showing the viewing chords (left), and optics, filter, and detector setup used in simultaneous D_α and NIR-emission measurements.

Emission from the dissociation of the deuterium molecule is likely the primary contaminant in visible bremsstrahlung measurements.¹² During dissociation, the upper radiating electronic level of D_2 is bound and the lower level is unbound on a repulsive molecular potential curve.^{13,14} The steep unbound potential curve¹⁵ spreads out the radiation over a vast range of wavelengths, leading to the observed continuum ranging from below 200 nm to almost 600 nm. This is consistent with the results published by Marmor *et al.*, where increased levels of broadband visible emission occur with puffs of diatomic molecules (D_2 or N_2), with no corresponding jump in emission for a helium puff.⁷ MST is fueled by introducing molecular deuterium at the plasma boundary (puffing and/or wall recycling), making the radiation from its dissociation an unfortunate artifact, and rendering impossible a visible bremsstrahlung measurement.

A study of the MST spectrum indicates that a region well suited for a bremsstrahlung continuum measurement lies in the NIR,¹² where emission from atomic and molecular deuterium lines, recombination, and molecular dissociation are all minimal. Closely spaced emission lines of helium, boron, carbon, nitrogen, oxygen, and aluminum barrage the ultraviolet and visible spectrum, but line radiation at 1040 nm is inconsequential. Figure 3 shows the measured NIR spectrum in MST, along with the bremsstrahlung expected for $Z_{\text{eff}}=2$ (solid line) and the wavelength response of the NIR detectors (dashed lines). The continuum appears noisy, as the measurement is near the wavelength cutoff of the CCD detector used.

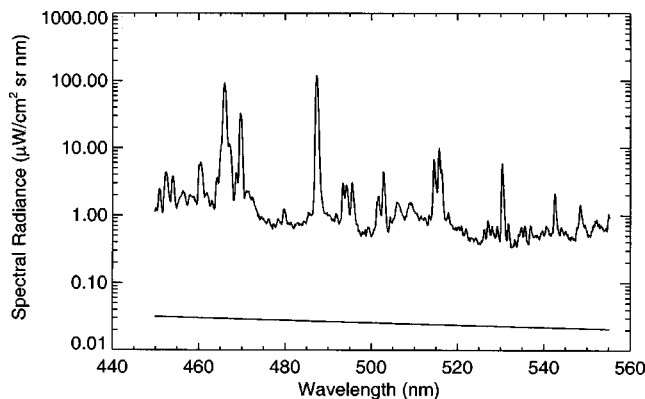


FIG. 2. The measured spectrum (near 500 nm) in MST and the bremsstrahlung expected for $Z_{\text{eff}}=2$ (solid line at the bottom).

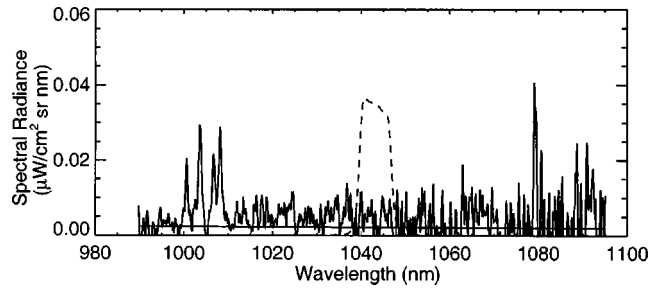


FIG. 3. The measured spectrum (near 1040 nm), bremsstrahlung expected for $Z_{\text{eff}}=2$ (solid), and the wavelength response function of the NIR-filtered photodiode detectors (dashed).

Deuterium and helium lines well above the background observed at both longer (1078, 1090 nm) and shorter (1003, 1009 nm) wavelengths indicate that there are no significant lines in the collection range, although there are allowed transitions from Cl , NI , and OII (low charge state MST impurities). Other contributors to the continuum (mainly due to neutral deuterium and non-fully-stripped ions) complicate, but do not prohibit, an NIR bremsstrahlung measurement.

An electron interacting with a neutral atom leads to continuous emission in a fashion similar to $e-i$ bremsstrahlung.¹⁶ As the free electron impinges on the neutral atom, it penetrates the outer electronic cloud, is subjected to a partially screened Coulomb force, and is accelerated. This proves to be a significant source of NIR light in MST, and makes the measured emissivity inconsistent with reasonable Z_{eff} bremsstrahlung.

The $e-n$ bremsstrahlung emissivity is calculated following the developments of Park¹⁷ and of Dalgarno and Lane.¹⁸ The spectral emission coefficient (in $W/cm^3/sr/nm$) is

$$\epsilon_{e-n}(\lambda) = \frac{hc}{4\pi\lambda} n_0 n_e \left(\int_{hc/\lambda}^{\infty} v \frac{d\sigma_v(E)}{dv} \frac{dv}{d\lambda} f(E) dE \right) \equiv n_e n_0 f_{e-n}(n_e, T_e), \quad (3)$$

where n_0 is the neutral density, v is the initial velocity of the electron, integration is over the electron energy distribution $f(E)$ starting at the energy of the photon of interest, and $d\sigma_v(E)/dv$ is the neutral bremsstrahlung emission cross section. It is possible to cast the $e-n$ bremsstrahlung emissivity at a given wavelength [Eq. (3)] as the product of $n_e n_0$ and a function $f_{e-n}(n_e, T_e)$, where f_{e-n} carries all the relevant information of the radiative process. Similarly, the D_α line intensity is described by

$$\gamma_{D_\alpha} = \frac{hc}{4\pi\lambda} n_e n_0 \langle \sigma v \rangle_{\text{exc}}(n_e, T_e) \equiv n_e n_0 f_{D_\alpha}(n_e, T_e), \quad (4)$$

where $\langle \sigma v \rangle_{\text{exc}}$ is the electron impact excitation reaction rate.¹⁹ It is thus clear that at a given electron density and temperature, the D_α emission is proportional to $e-n$ bremsstrahlung, or $\epsilon_{e-n} = \alpha \gamma_{D_\alpha}$, where the proportionality constant is simply

$$\alpha(n_e, T_e) = \frac{f_{e-n}(n_e, T_e)}{f_{D_\alpha}(n_e, T_e)}. \quad (5)$$

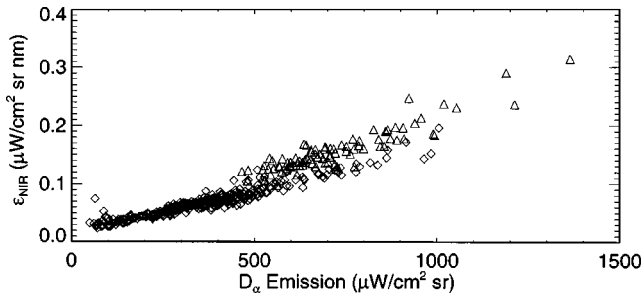


FIG. 4. Emission at 1040 nm vs D_α emission, separated by electron density. The data represented by diamonds are for low density (average $\bar{n}_e = 1 \times 10^{13} \text{ cm}^{-3}$), while the triangles represent higher density discharges (average $\bar{n}_e = 2 \times 10^{13} \text{ cm}^{-3}$). As expected, the y-intercept is higher for the higher density discharges, with a similar slope in each set of data.

As α is a function of electron density and temperature, it will not be constant over the line of sight in a chord-integrated measurement. The amount of light collected, however, is weighted by the neutral density profile which is measured to be poloidally asymmetric and extremely edge-localized in the MST. Peak values of n_0 are on the order of 10^{13} cm^{-3} , and the profile drops by more than an order of magnitude over the first few centimeters inside the plasma boundary.²⁰ Approximating the neutral density as a δ function at the edge [$n_0(\rho) = N_0 \delta(\rho - a)$] clearly illustrates that the proportionality of e-n bremsstrahlung to D_α emission is preserved in the chord-integrated measurement. The measured D_α emission is the line integral of Eq. (4):

$$M_{D_\alpha} = N_0 n_e(a) f_{D_\alpha}(a), \quad (6)$$

the integrated e-n bremsstrahlung is similarly found from Eq. (3):

$$M_{e-n} = N_0 n_e(a) f_{e-n}(a), \quad (7)$$

and the two quantities are again proportional.

As the continuous NIR emission is the sum of e-i and e-n bremsstrahlung ($\epsilon_{1040} = \epsilon_{e-i} + \alpha \gamma_{D_\alpha}$), a linear relationship between the measured NIR emission and the measured D_α emission is predicted:

$$M_{1040} = \int_0^L \epsilon_{e-i} dl + \bar{\alpha} \int_0^L \gamma_{D_\alpha} dl = B + 2, \quad (8)$$

where B and M_{D_α} are the line-integrated e-i bremsstrahlung and D_α emission, respectively, and $\bar{\alpha} = \alpha(a)$ is the chord-averaged proportionality factor. The δ function approximation of the neutral density and the assumption of two primary components of NIR emission are consistent with the data. Figure 4 shows the expected linear behavior between NIR and D_α emission; the slope is $\bar{\alpha}$ and the y-intercept is the measured e-i bremsstrahlung. The data represent line-integrated measurements of the emission during a narrow time window [with low magnetohydrodynamic (MHD) activity] in a discharge. Experiments repeated in helium discharges confirm that the NIR pollution is proportional to neutral density (monitored by a HeI line at 587 nm) as opposed to deuterium lines or molecular emission.

Quantitative prediction of the e-n bremsstrahlung emissivity is possible with measured electron and neutral density

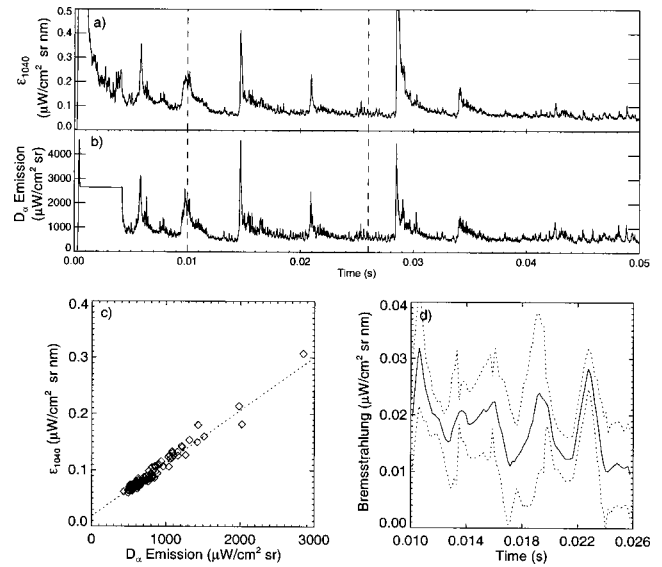


FIG. 5. (a) NIR and (b) D_α signals vs time. (c) NIR vs D_α emission is plotted for time points between $t = 0.010$ and 0.026 s and (d) the time-resolved bremsstrahlung signal, with uncertainty upper and lower bounds in dotted lines.

profiles and tabulated cross sections for deuterium. The predicted slope (assuming e-n bremsstrahlung as the only contaminant) is about $2 \times 10^{-5} \text{ nm}^{-1}$, while measurements are higher but show order-of-magnitude agreement. The cause of the higher slope is very likely other sources of emission that are proportional to neutral density; continuous emission from free-bound interactions (leading to negative hydrogen ions)²¹ and deuterium-deuteron charge exchange²² are possible in the low-temperature, high-neutral-density region of the plasma. The important point is that the emission arises from interactions with neutral particles, and is therefore edge localized and proportional to D_α emission.

III. NIR BREMSSTRAHLUNG MEASUREMENT

The e-i bremsstrahlung signal is determined by fitting a line to the NIR versus D_α emission graph and extrapolating to zero neutral density to find the y-intercept. Figure 5 shows typical signals from the NIR and D_α detectors; every variation in the D_α signal appears in the NIR signal, as expected. Also shown is a slower (~ 6 kHz) plot of the NIR versus D_α emission between $t = 0.010$ and 0.026 s and the deduced e-i bremsstrahlung signal. Dynamically fitting a line to nine data points determines the slope and intercept as functions of time. During periods of slowly varying electron density and Z_{eff} (1.5 ms averaging is inherent in this analysis), the intercept is the e-i bremsstrahlung emissivity. This signal is typically noisy, with uncertainty primarily due to error in extrapolating to zero on the x-axis, but is improved by averaging data from many similar discharges.

The e-i bremsstrahlung ($\sim 0.02 \text{ } \mu\text{W/cm}^2/\text{sr/nm}$) is only a small fraction of the measured emission (0.05 – $0.2 \text{ } \mu\text{W/cm}^2/\text{sr/nm}$). The signal-to-pollution ratio thus ranges from about 10% to 40%. In enhanced-confinement MST plasmas, the neutral particle density and D_α emission are greatly reduced, the signal-to-pollution ratio is typically greater than 50%, and the extrapolation uncertainty is de-

creased. Removal of the neutral contribution to the continuous emission as described above combines all other unchecked contaminants into the e–i bremsstrahlung measurement. Enhanced bremsstrahlung from neutral and non-fully-stripped impurity atoms²³ are not separately measured, but can contribute significantly to the emission. Furthermore, very dim lines (below the resolution of the spectrometer, data in Fig. 3) from the low-charge-state impurities likely contribute a small amount of light. Fortunately, these sources of light are limited to the extreme edge region (where neutral and singly ionized impurities may exist) and are small compared to e–i bremsstrahlung in the core of the hot plasma. Since the non-neutral contaminant is small compared to core e–i bremsstrahlung, it is possible to invert the data to determine the emissivity profile. It is impossible to accurately invert these data without correcting for the e–n radiation, as the pollutant magnitude is greater (often much greater) than the core bremsstrahlung, and the proportionality to neutral density makes the emission extremely edge-peaked and poloidally asymmetric.

With the measured e–i bremsstrahlung and profiles of electron temperature and density, Z_{eff} is deduced. The result in a certain set of MST plasmas, [$T_e(0) \sim 800$ eV, $n_e(0) \sim 1 \times 10^{13}$ cm⁻³, produced without prior boronization of the aluminum vacuum vessel] is a core Z_{eff} of 4.6 ± 0.7 . This result is corroborated by Fokker–Planck modeling, in which the measured x-ray flux (10–100 keV) matches the prediction based on the measured Z_{eff} and electron transport properties.²⁴ In standard-confinement plasmas with significantly lower electron temperature, removal of the pollutant emission from neutrals does not lead to a well-determined Z_{eff} , as emission from low-charge-state impurities (primarily C) obscures the measurement of e–i bremsstrahlung. Current work includes investigation of longer wavelengths (near 1170 or 1600 nm), where carbon lines are completely absent. The silicon photodiodes are insensitive to these wavelengths, and are replaced with InGaAs photodiodes having excellent sensitivity at these wavelengths. These measurements will proceed following an infrared spectral survey which should identify promising line-free regions.

IV. SUMMARY

In summary, the consideration of neutral bremsstrahlung and molecular dissociation may shed some light on the difficulties that abound in absolute bremsstrahlung measurements. The dissociating deuterium molecule radiates in the wavelength range of standard visible bremsstrahlung measurements. Emission from electron–neutral bremsstrahlung (and likely other neutral processes) is significant in the NIR at low electron density.

Removal of the neutral emission has enabled an NIR measurement of electron–ion bremsstrahlung at electron densities as low as $n_e \sim 1 \times 10^{13}$ cm⁻³ in the MST. The line-integrated D_α emission is proportional to the pollutant emis-

sion, and a fraction of this signal is removed from the total NIR emission (from the same sample volume) to extract the e–i bremsstrahlung. Accurate extraction of Z_{eff} is limited to the high temperature range of MST as low temperatures allow significant populations of low-charge-state impurities that enhance the continuous emission and increase the likelihood of impurity line pollution. In MST, uncorrected neutral contamination to e–i bremsstrahlung typically leads to an apparent enhancement of Z_{eff} by a factor of 2 to 4, but can briefly be as high as 10 with the high neutral density observed at large amplitude MHD events. In other devices with higher electron density and lower neutral density, the enhancement of the deduced Z_{eff} due to pollution from neutrals should be smaller, but perhaps not negligible.

ACKNOWLEDGMENTS

The authors are indebted to a large group of collaborators on this project, particularly D. Whyte and J. Lawler for useful discussions of bremsstrahlung and atomic physics. Thanks also to T. Biewer for leading a fully-diagnosed experimental campaign; and S. Castillo and S. Gerhardt for development of the diagnostic. This work is supported by the U.S. Department of Energy and the Oak Ridge Institute for Science and Education Fusion Energy Science Fellowship Program.

- ¹K. Kadota, M. Otsuka, and J. Fujita, *Nucl. Fusion* **20**, 209 (1980).
- ²A. T. Ramsey and S. L. Turner, *Rev. Sci. Instrum.* **58**, 1211 (1987).
- ³M. T. Fall, Ph.D. thesis, L'Université Paris xi Orsay, 1991.
- ⁴H. Weisen, D. Pasini, A. Weller, and A. W. Edwards, *Rev. Sci. Instrum.* **62**, 1531 (1991).
- ⁵N. J. Peacock, K. D. Lawson, R. Barnsley, and H. Chen, *Rev. Sci. Instrum.* **71**, 317 (1999).
- ⁶D. G. Whyte *et al.*, *Nucl. Fusion* **38**, 387 (1999).
- ⁷E. S. Marmar, R. L. Boivin, R. S. Granetz, J. W. Hughes, and B. Lipschultz, *Rev. Sci. Instrum.* **72**, 940 (2001).
- ⁸B. Grek, J. Bartolick, and D. Johnson, *Rev. Sci. Instrum.* **63**, 4627 (1992).
- ⁹H. Röhr and K. H. Steuer, *Rev. Sci. Instrum.* **59**, 1875 (1988).
- ¹⁰J. J. Rommers, R. Behn, B. P. Duval, S. Franke, and Z. A. Pietrzyk, *Proceedings of the International Symposium on Laser-Aided Plasma Diagnostics* (Doorwerth, The Netherlands, 1997), pp. 235–240.
- ¹¹L. Carraro, S. Costa, M. E. Puiatti, F. Sattin, P. Scarin, and M. Valisa, *Plasma Phys. Controlled Fusion* **42**, 731 (2000).
- ¹²J. K. Anderson, Ph.D. thesis, University of Wisconsin-Madison, 2001.
- ¹³J. Lawler (private communication).
- ¹⁴E. F. McCormack, S. T. Pratt, P. M. Dehmer, and J. L. Dehmer, *J. Chem. Phys.* **98**, 8370 (1993).
- ¹⁵T. E. Sharp, *Atomic Data* **2**, 119 (1971).
- ¹⁶G. Bekefi, *Radiation Processes in Plasmas* (Wiley, New York, 1966).
- ¹⁷J. Park, I. Henins, H. W. Herrmann, and G. S. Selwyn, *Phys. Plasmas* **7**, 3141 (2000).
- ¹⁸A. Dalgarno and N. F. Lane, *Astrophys. J.* **145**, 623 (1966).
- ¹⁹L. C. Johnson and E. Hinnov, *J. Quant. Spectrosc. Radiat. Transf.* **13**, 333 (1973).
- ²⁰N. E. Lanier, Ph.D. thesis, University of Wisconsin-Madison, 1999.
- ²¹W. G. Graham, *Plasma Sources Sci. Technol.* **4**, 281 (1995).
- ²²A. M. Ermolaev, A. A. Mihajlov, L. M. Ignjatovic, and M. S. Dimitrijevic, *J. Phys. D* **28**, 1047 (1995).
- ²³V. D. Kirillov, B. A. Trubnikov, and S. A. Trushin, *Sov. J. Plasma Phys.* **1**, 117 (1975).
- ²⁴R. O'Connell (private communication).